Electronic Supplementary Material (ESI) for Journal of Materials Chemistry A.

Supporting Information

Experimental Details

Catalyst Preparation. Ruthenium chips (99.9%, Myojokinzoku Inc.) and Cerium chips (99.9%, Sigma Aldrich Corporation) were used as starting materials. Ru and cerium chips were melted in arc melting furnace to prepare Ru_2Ce alloy precursors. The alloy was then crushed with mortar and sieved to get powder of 50 μm - 60 μm. Next, heat treatments (promotion of nanophase separation) were conducted at in gas mixture (1 vol% O_2, 2 vol% CO, and balanced by Ar gas; 60 mL min^{-1}) at 600 ^oC with heating rate of $1^oC\ min^{-1}$ for 12 hours. The obtained Ru#CeO_2 nanocomposite was then immersed in H_2SO_4 (12M) for 6h to obtain the nanoporous Ru materials. The np-Ru corresponds to the Ru#CeO_2 nanocomposite leached for 6 hours. Ru powder (for comparison) was prepared by reducing $RuCl_3$ in a stream of H_2 gas (H_2 : Ar = 5% : 95%) at 400ºC for 3 hours.

Catalyst characterization. Powder XRD was collected with PANalytical X'Pert PRO (Cu Kα, 45 kV, 30 mA). Samples were scanned in the 2θ range from 10^o to 100^o in steps of $0.0857^o\ s^{-1}$. TEM images and EDS mapping were obtained using JEM-ARM200F-Green (Acc. voltage 200 kV, Emission: 101 μA) and JEOL JED respectively. Ru#CeO_2 nanocompite sample were trimmed to the thickness of 70 nm with FIB (JEM-9320FIB) prior to TEM observation. FE-SEM attached with EDX detector (Hitachi SU-8230) was also used with scanning voltage set to be 5kV. N_2 physisorption was conducted with Micromeritics ASAP 2010 analyzer at 77 K to get the isotherm adsorption/desorption isotherm, Brunauer-Emmett-Teller (BET) surface areas and Barrett, Joyner, and Halenda (BJH) pore distribution. Degassing at 423 K for 3 hours was carried out to eliminate surface impurities prior to the analysis.

Electrochemical measurement. Electrochemical investigation was carried out using three-electrode cell equipped with CH Instrument (CHI 842B) potentiostat. A mixture of distilled water (398 µl), propanol (100 µl), Nafion (2 µl), and catalyst (2.5 mg) was prepared and sonicated for 10 minutes to obtain an ink. The ink (5 µl) was then dropped to coat the working electrode (glassy carbon electrode) and left to dry in a furnace at room temperature. The prepared working electrode was then placed in an electrochemical cell together with a counter electrode (Pt wire, diameter = 1 mm) and a reference electrode (Ag/AgCl). All potentials were converted to RHE by adding a value of 0.195+0.059pH (reference value at 25°C). The electrochemical studies for HER were conducted in 0.5 M H_2SO_4 solution under argon, at 25°C and under continuous stirring. Counter electrode of graphite was used as control. In addition, HER with perchloric acid ($MClO_4$) 0.1M as electrolyte was also done as control. Cu underdeposition was adopted to calculate turnover frequency (TOF) as per suggested from few literatures. [1,2] TOF=I/(2Fn) where I is the current (A) during HER linear sweep measurement, F is the Faraday constant (C mol^{-1}), n is the number of active sites (mol). Since $n=Q_{Cu}/2F$, TOF calculation is simplified as $TOF = I/Q_{Cu}$. Q_{cu} was obtained from integration of curve related to Cu monolayer stripping only.

The electrochemical surface area (ESCA) was quantified by measuring the double-layer capacitance by cyclic voltammetry (CV). The CV curves in a non-faradaic region (-0.2 to 0.34 V) were plotted as a function of various scan rates. The double layer capacitance (C_{dl}) was evaluated from the slope of the linear regression between the current differences in the middle of the potential window of CV curves versus the scan rates (20, 40, 60, 80, 100 mV/s; see Figure S19) as $i = v.C_{dl}$. Based on the literature reported C_s values is generally materials, 0.035 mF cm^{-2} was considered for EASA calculation.[3–5] The ECSA value was obtained by dividing C_{dl}/C_s with the loading weight of the catalyst.[6] Electrochemical impedance spectra (EIS; Nyquist plot) at a potential of -0.4 V over the frequency range of 0.01 Hz–100 kHz was also carried out with 0.5 m H_2SO_4 solution as electrolyte and graphite as counter electrode. For stability evaluation, chronogalvanometry and chronoamperometric was done in 0.5 M H_2SO_4 solution. The former was done at +10 mA for 6 hours, while the latter was done for 1 hours and the current retention was recorded and plotted.

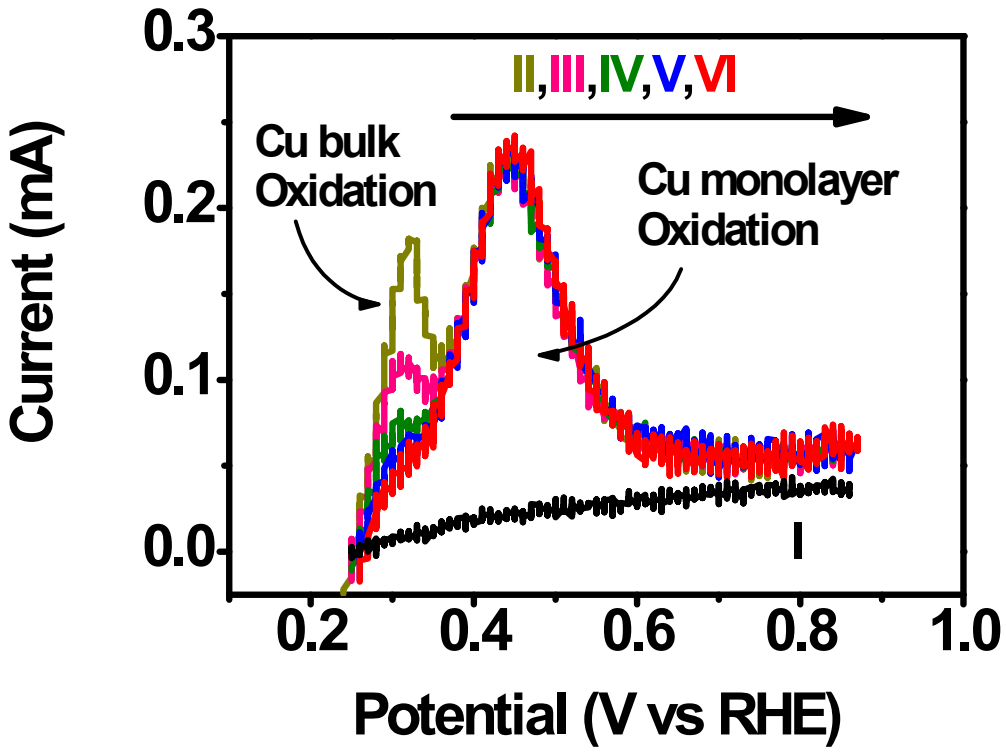

Figure S1: Copper under deposition of np-Ru. I corresponds to LSV in H_2SO_4, while II,III,IV,V,VI correspond to LSV in H_2SO_4 + 5mM $CuSO_4$ with underdeposition for 90s at potential of 0.245 V, 0.250 V, 0.255 V, 0.260 V, 0.265 V respectively.

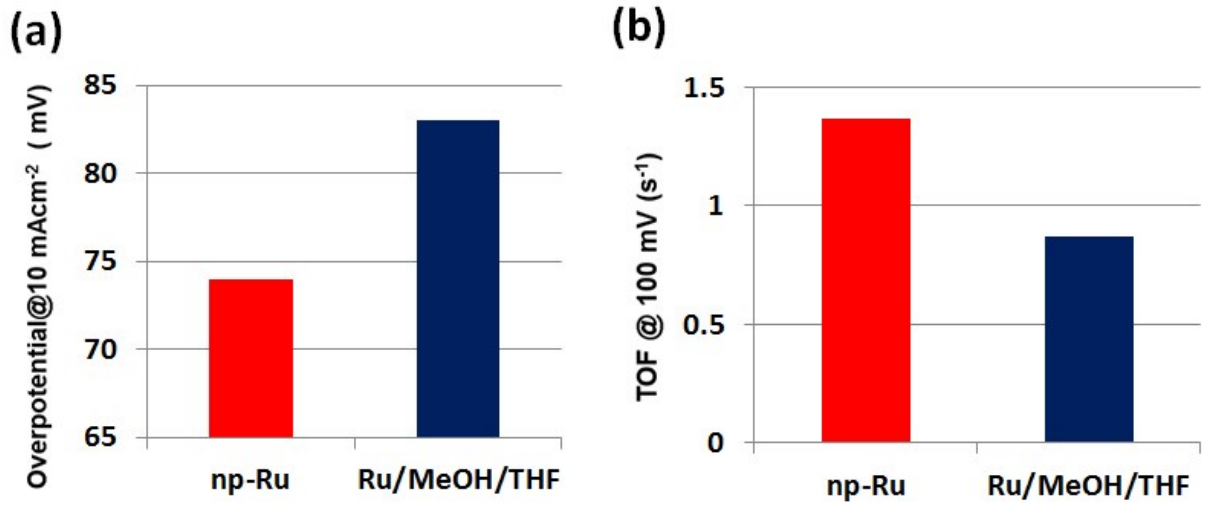

Figure S2: HER comparison between nanoporous metallic Ru of this work np-Ru (red) and previously reported Ru/MeOH/THF.[2] (a) Overpotential at 10 $mAcm^{-2}$ (b) TOF at 100 mV.

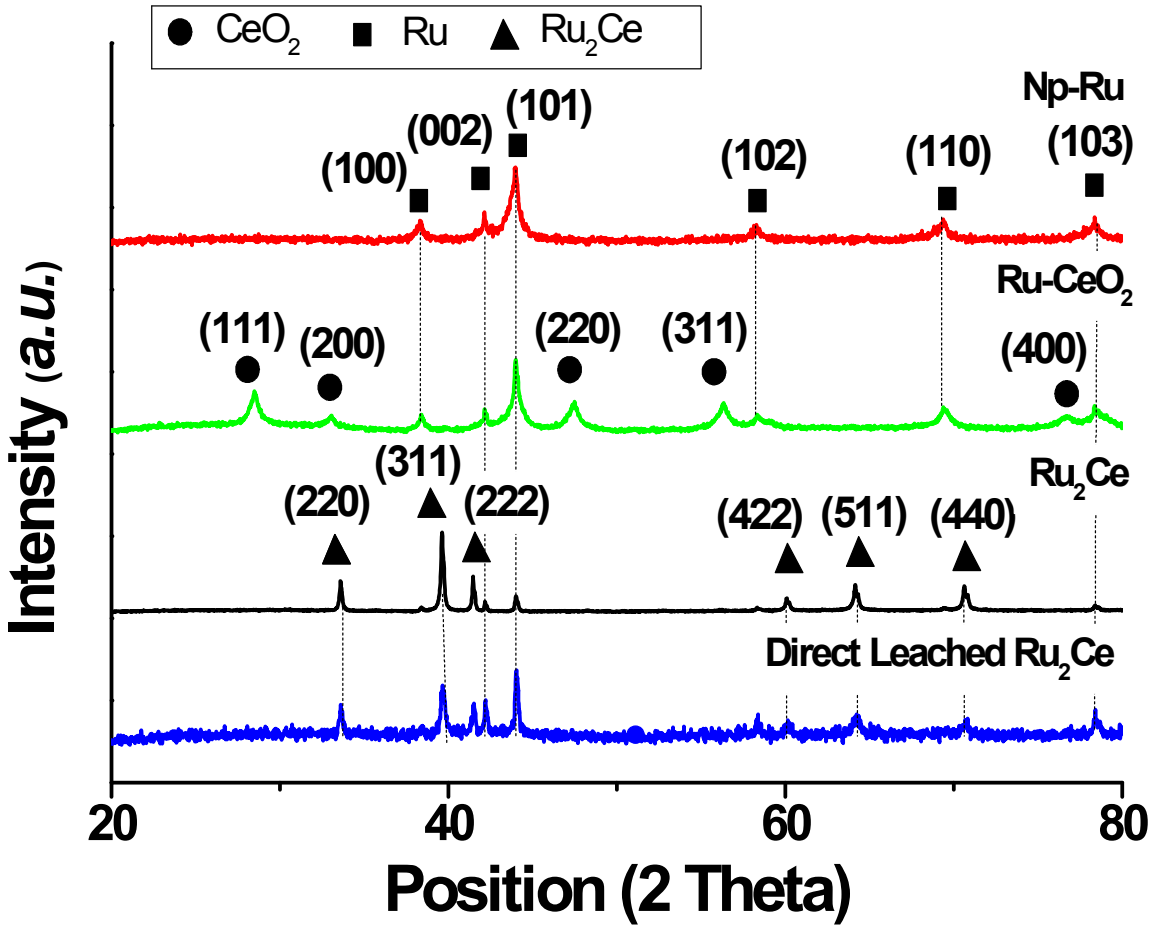

Figure S3: Powder X-Ray diffraction of Ru_2Ce precursor, Ru-CeO_2 nanocomposite, nanoporous Ru, and directly leached Ru_2Ce.[7]

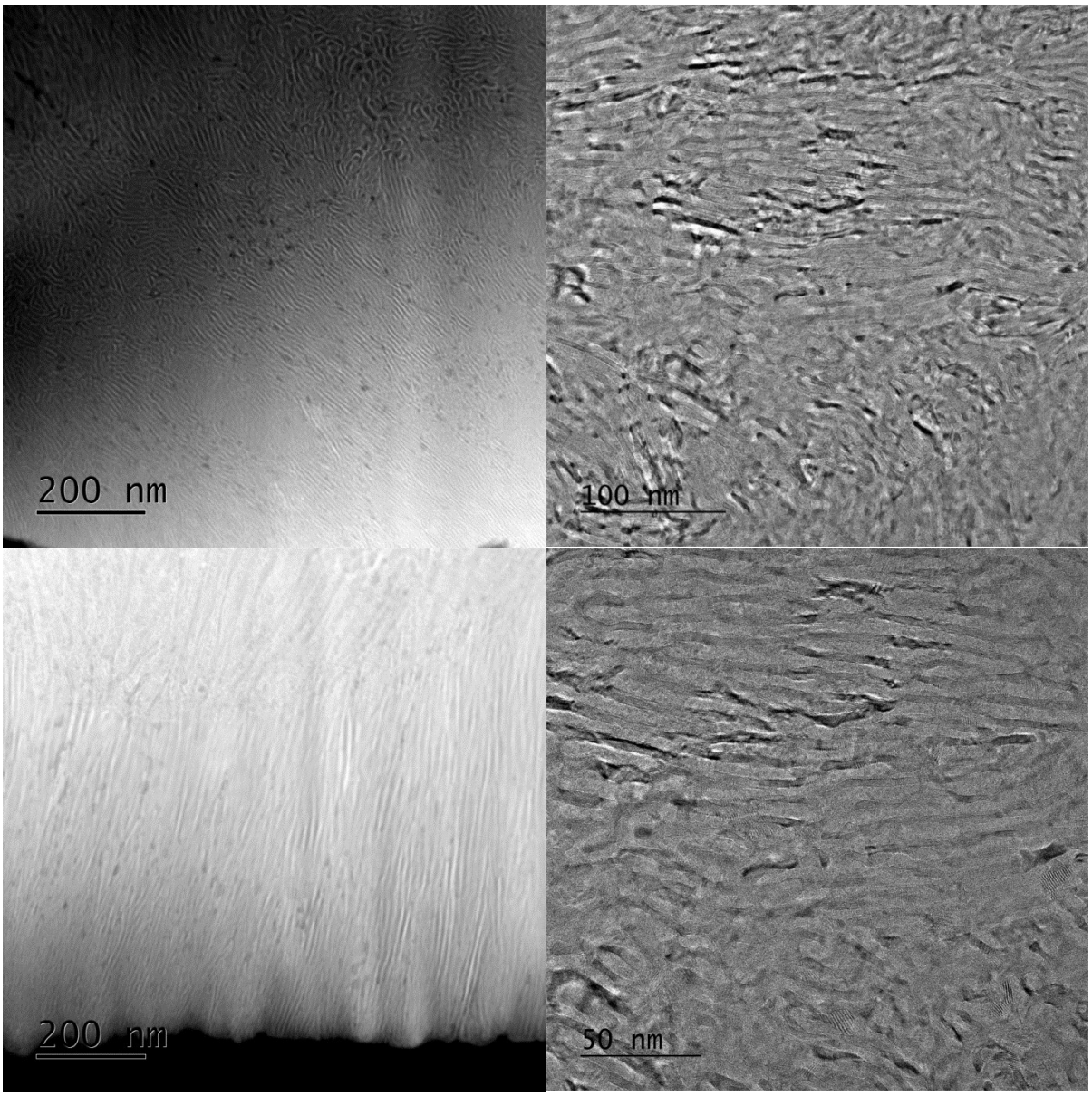

Figure S4. ADF-STEM images (left top and bottom) and TEM images (right top and bottom) of Ru-CeO_2 nanocomposite.

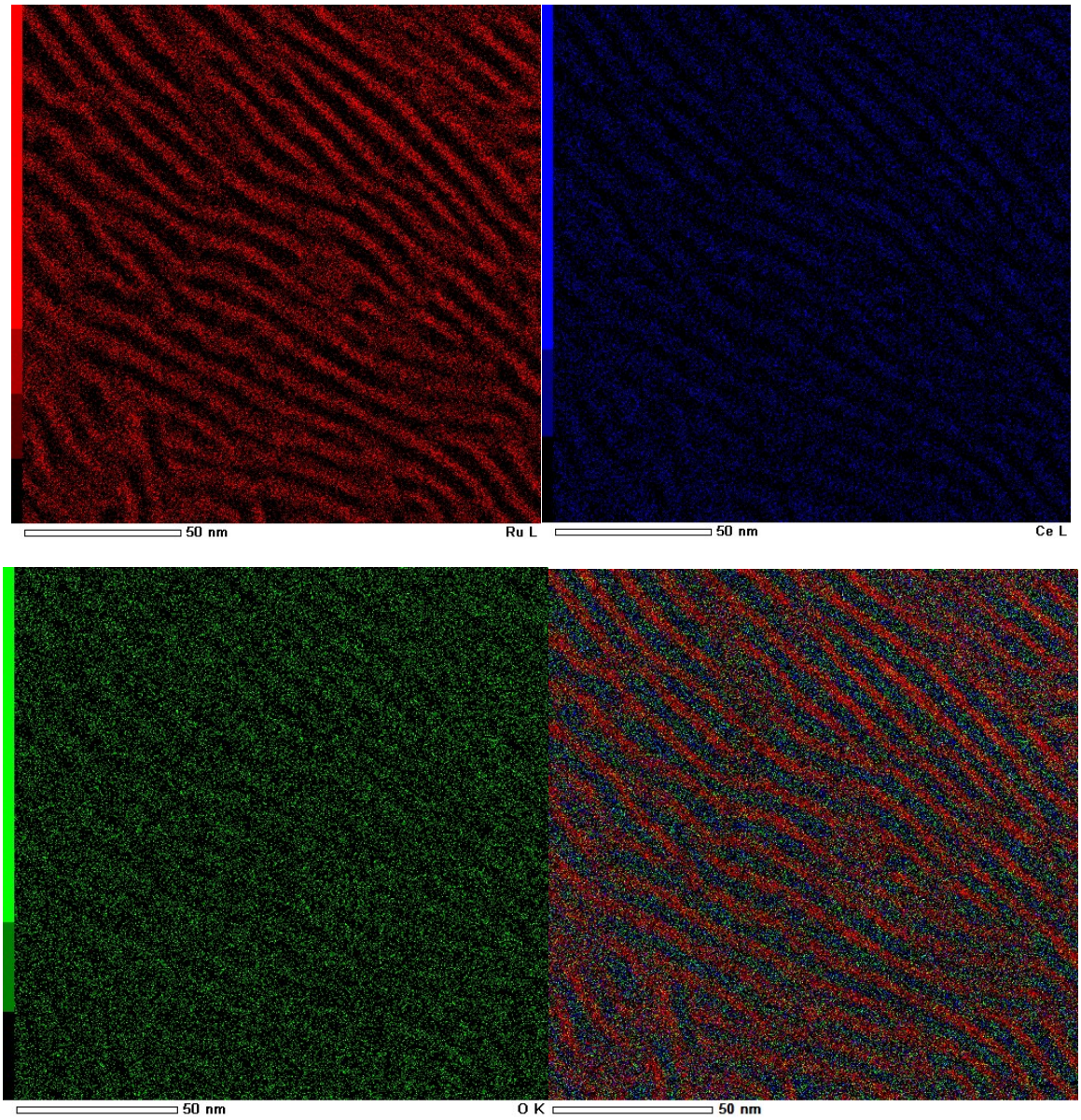

Figure S5. EDS elemental mapping of Ru-CeO_2 nanocomposite. Red = Ru, Blue = Ce, Green = O

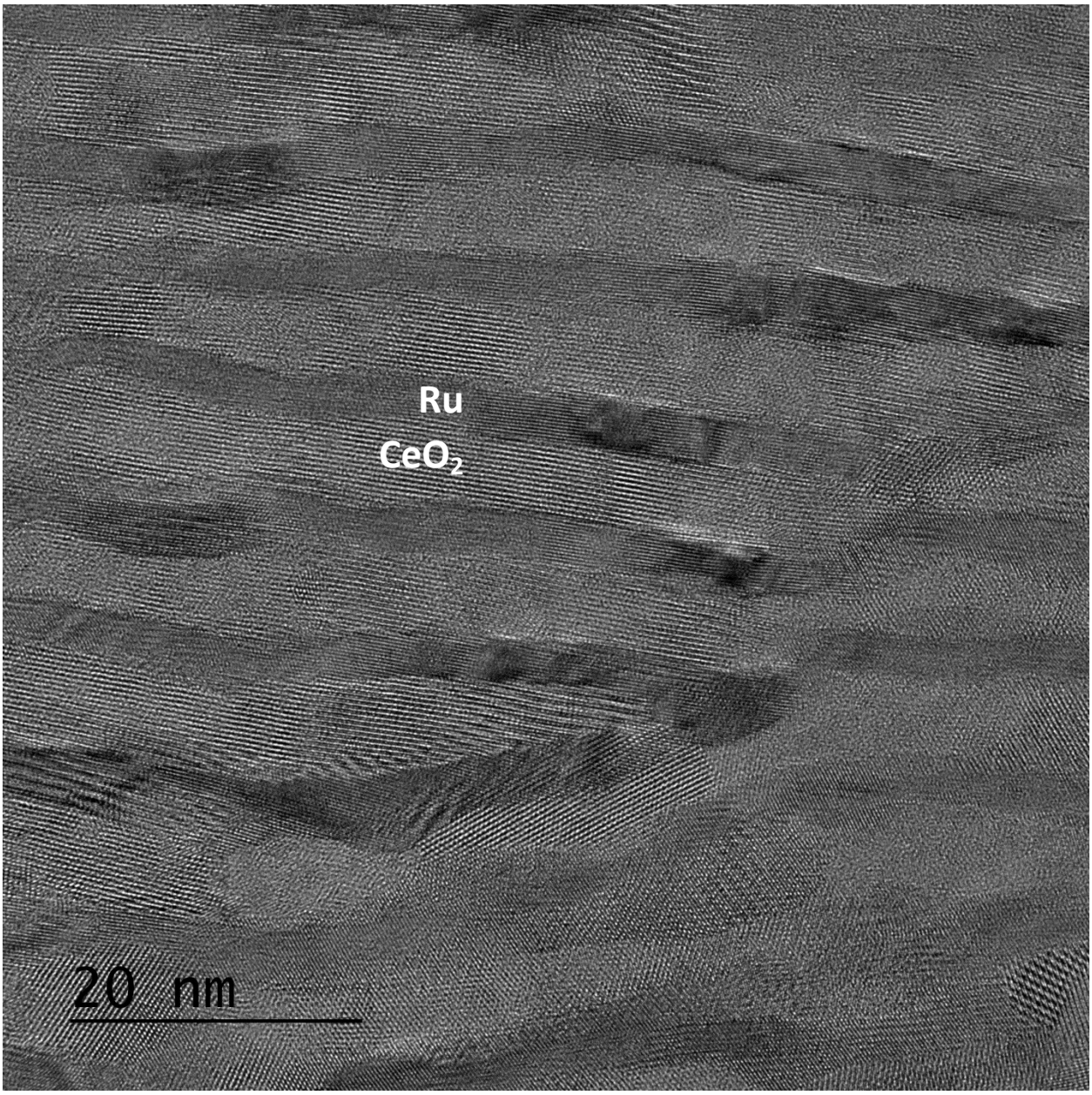

Figure S6. TEM image of Ru-CeO_2 nanocomposite. Ru and CeO_2 that are adjacent to each other is parallel

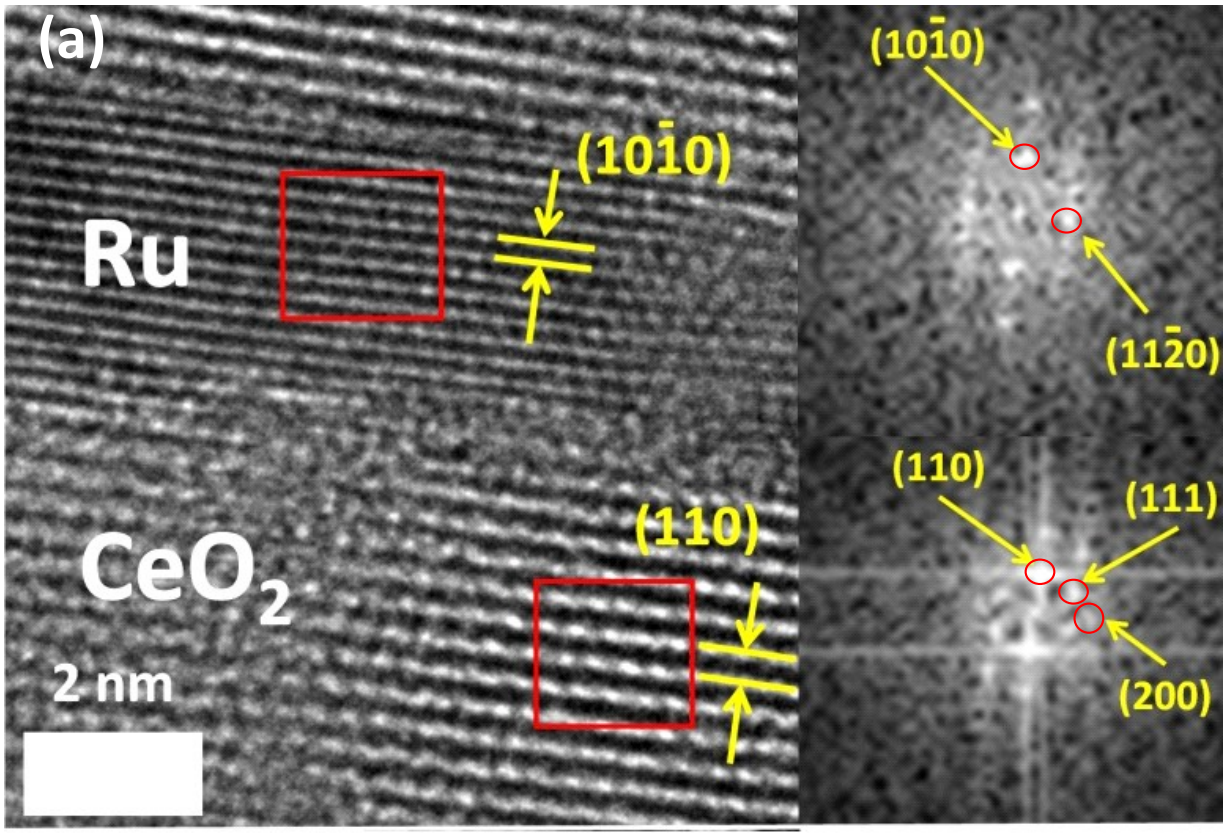

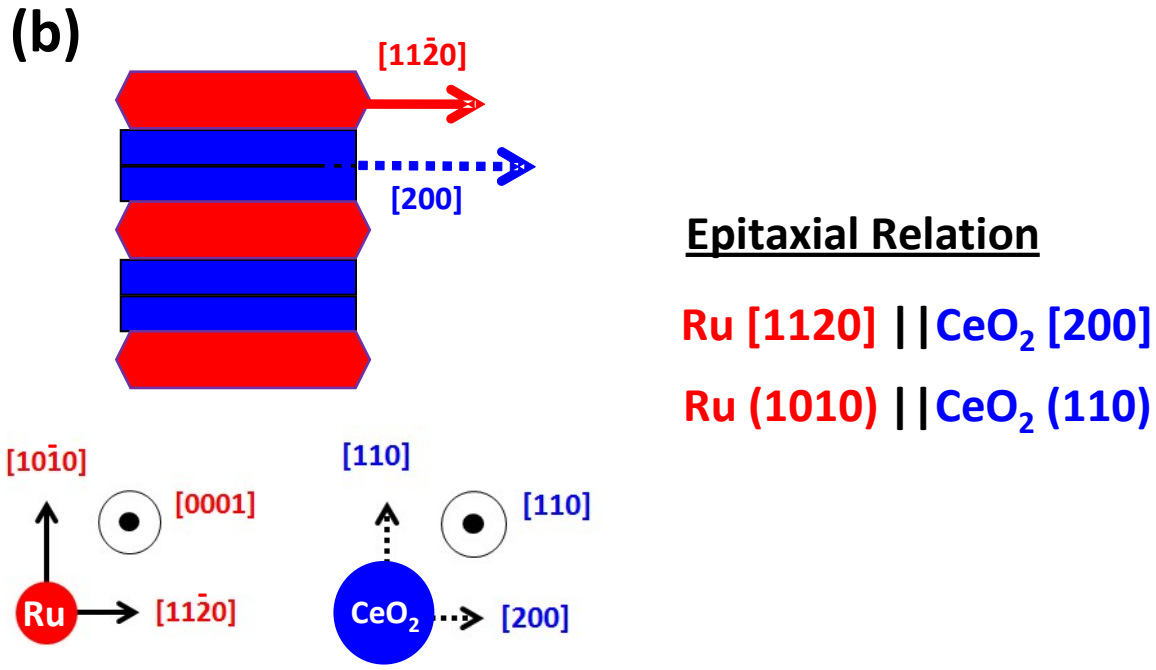

Epitaxial Relation

Ru [1120] ||CeO_2 [200]

Ru (1010) ||CeO_2 (110)

Figure S7. (a) TEM image and FFT analysis at Ru-CeO_2 interface, (b) Interface orientation development

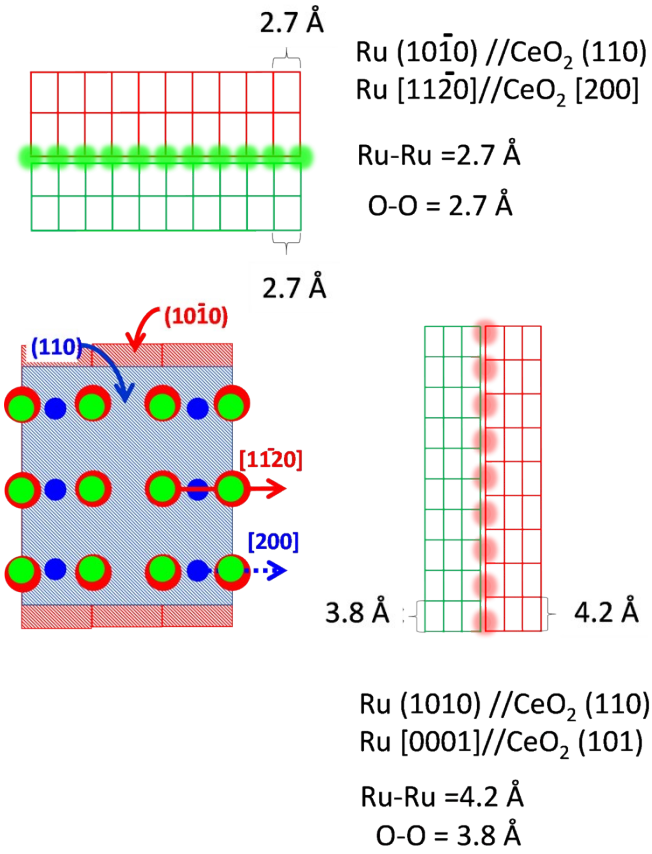

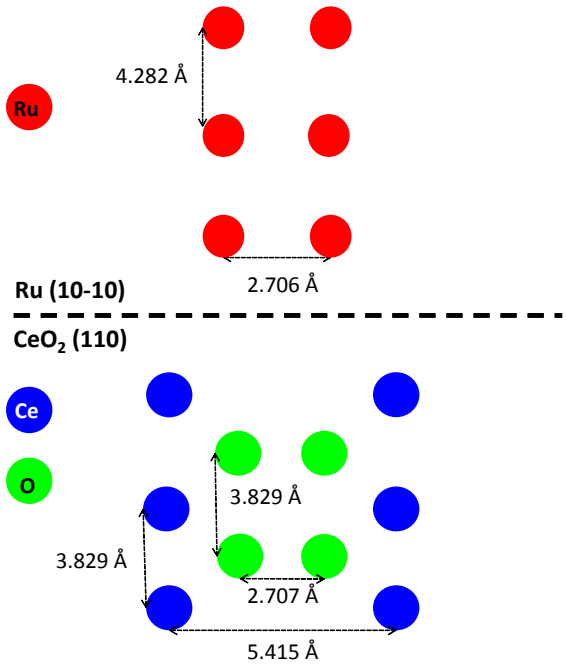

Figure S8. Lattice misfit at Ru-CeO_2 interface

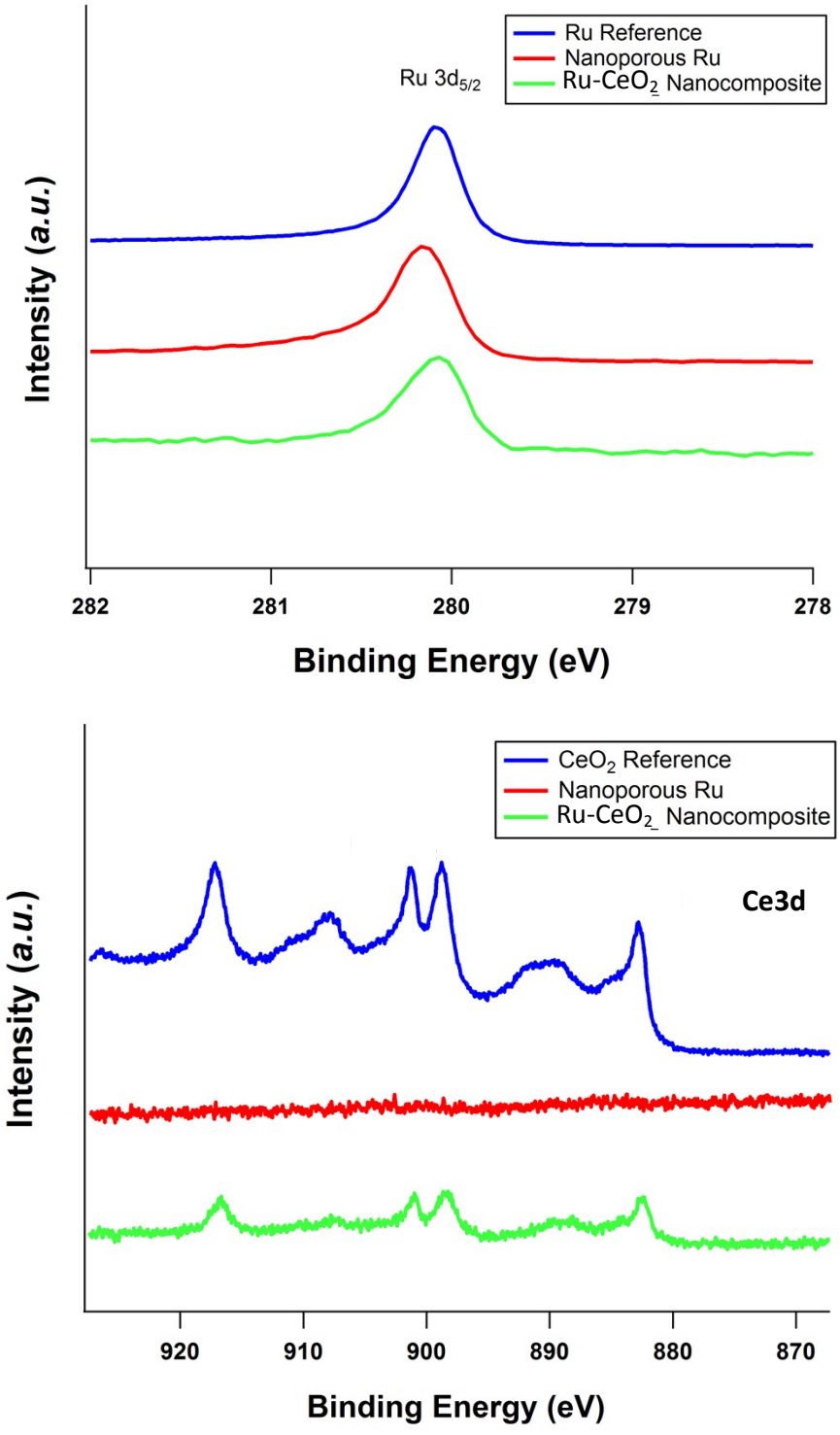

Figure S9: Hard X-Ray photoelectron spectra of Ru_2Ce precursor, Ru-CeO_2 nanocomposite, and nanoporous Ru referring to (a) Ru3d and (b) Ce3d orbital.[8,9]

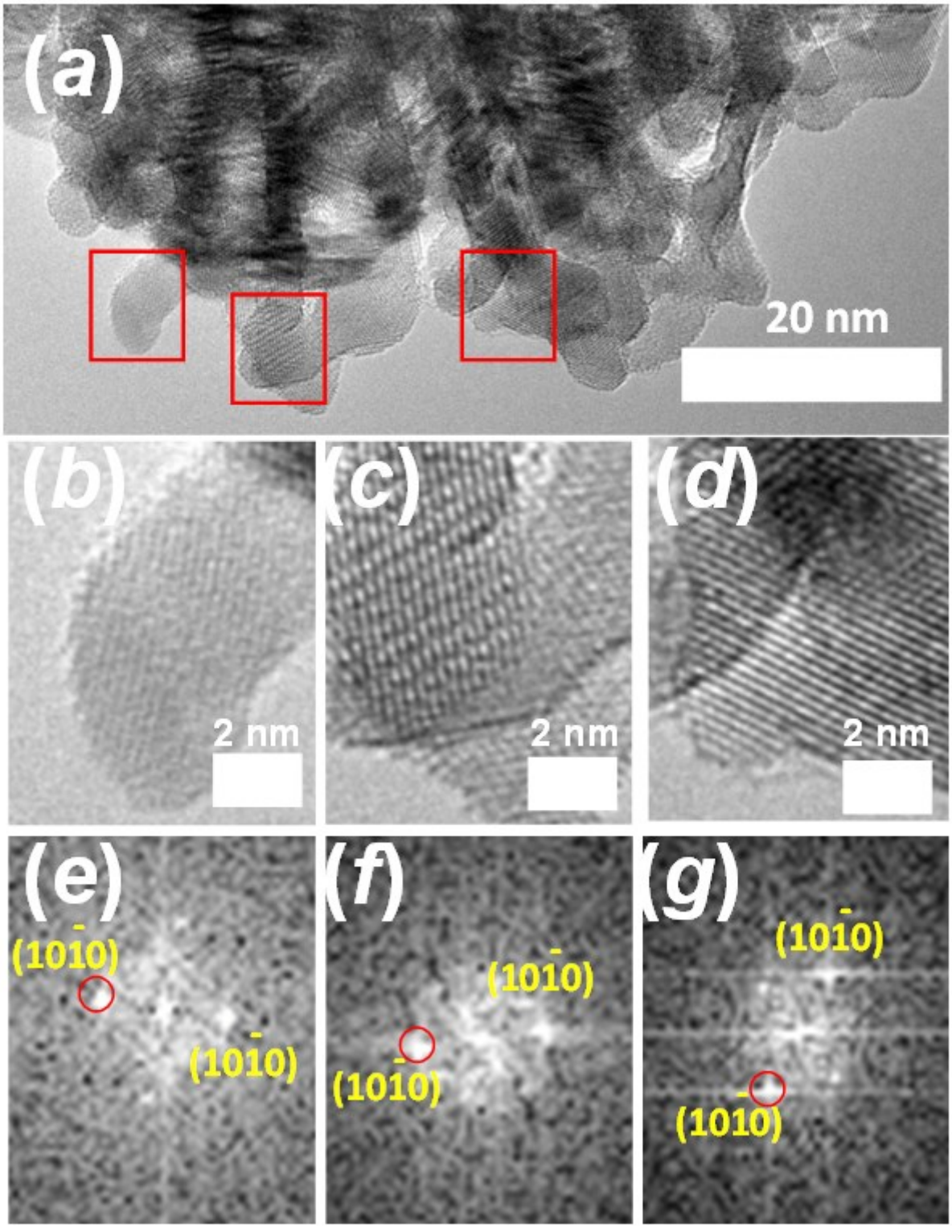

Figure S10. TEM image and the corresponding FFT patterns of np-Ru. (b)-(e), (c)-(f) and (d)-(g) are corresponded to each other.

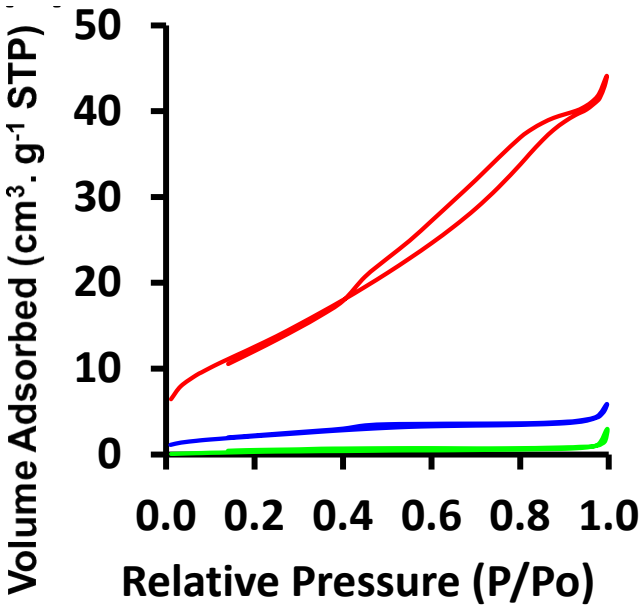

Figure S11: N_2 adsorption-desorption isotherm of Ru_2Ce precursor, Ru#CeO_2 nanocomposite, np-Ru, and directly leached Ru_2Ce precursor

N_2 physisorption was conducted and the adsorption-desorption isotherm was plotted. Np-Ru showed Type IV isotherm that is widely known for porous materials (Figure S10 – red) with the hysteresis that of Type H3 which represents slit-shaped or lamellar pores.[10] This is consistent with the developed Ru pattern observed in TEM images (Figure 1c,d). Isotherm of directly dealloyed Ru_2Ce was Type II isotherm disproving any possibility of nanoporous structure formation despite slight increase of volume adsorbed (Figure S10 – blue). BET (Brunauer-Emett-Teller) method is used to quantify specific surface area for comparison. Np-Ru specific surface area was significantly high with 48 m^2g^{-1} compared to directly dealloyed Ru_2Ce which was only 8 m^2g^{-1}. Further investigation by FESEM also visually showed that there was no formation of pores (Figure S9).

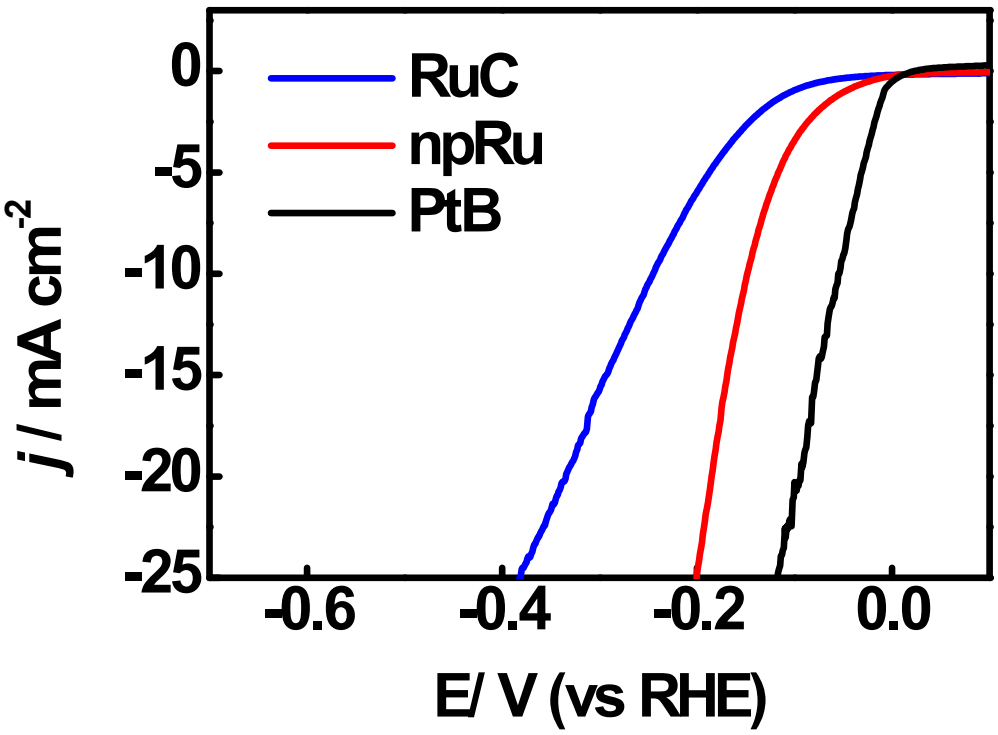

Figure S12: Linear-sweep voltammetry (LSV) profiles for np-Ru (red), Ru/C (blue) and Pt black (black) using graphite rod as counter electrode.

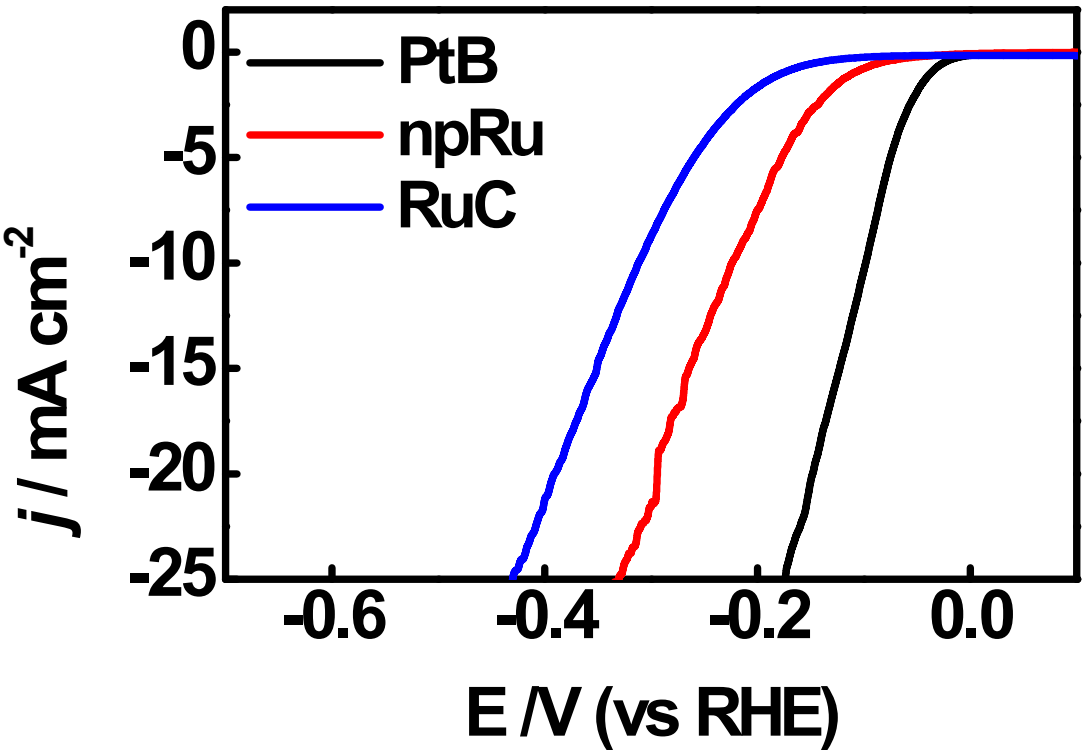

Figure S13: Linear-sweep voltammetry (LSV) profiles for np-Ru (red), Ru/C (blue) and Pt black (black) using graphite rod as counter electrode ($HClO_4$ (0.1 M) as electrolyte).

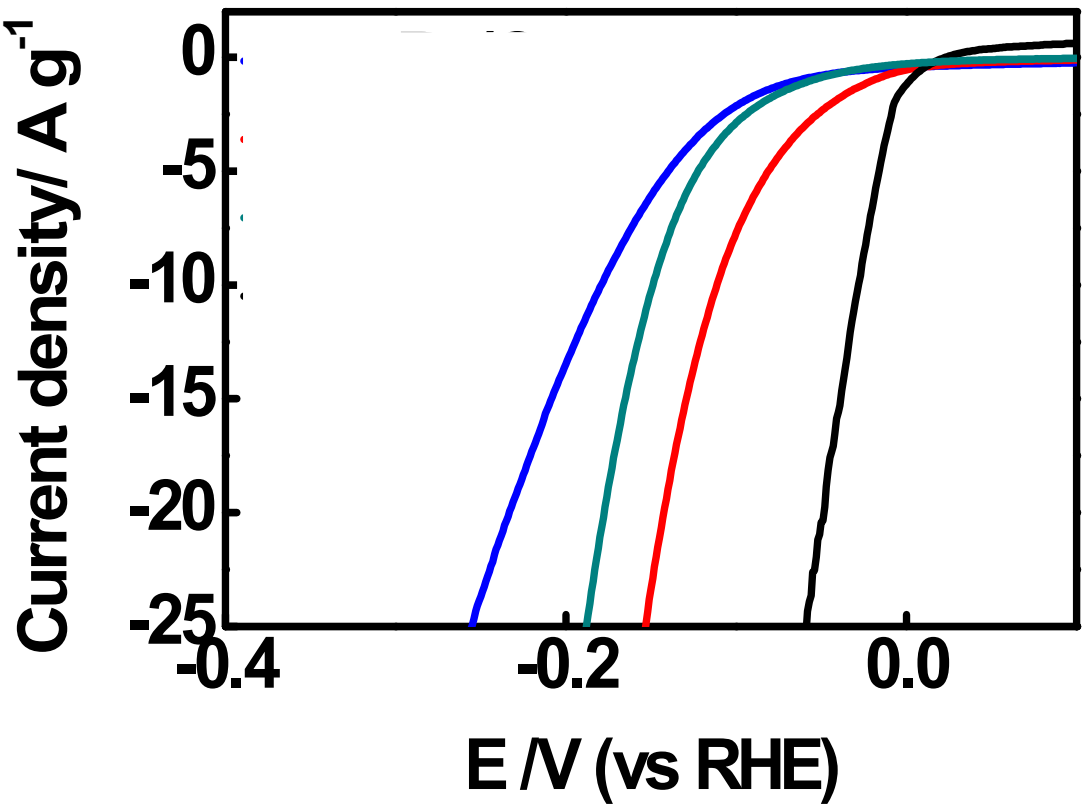

Figure S14: Linear-sweep voltammetry (LSV) profiles normalized with mass loading for np-Ru (red), Ru/C (blue), Ru (green) and Pt black (black) using graphite rod as counter electrode (H_2SO_4 (0.5 M) as electrolyte).

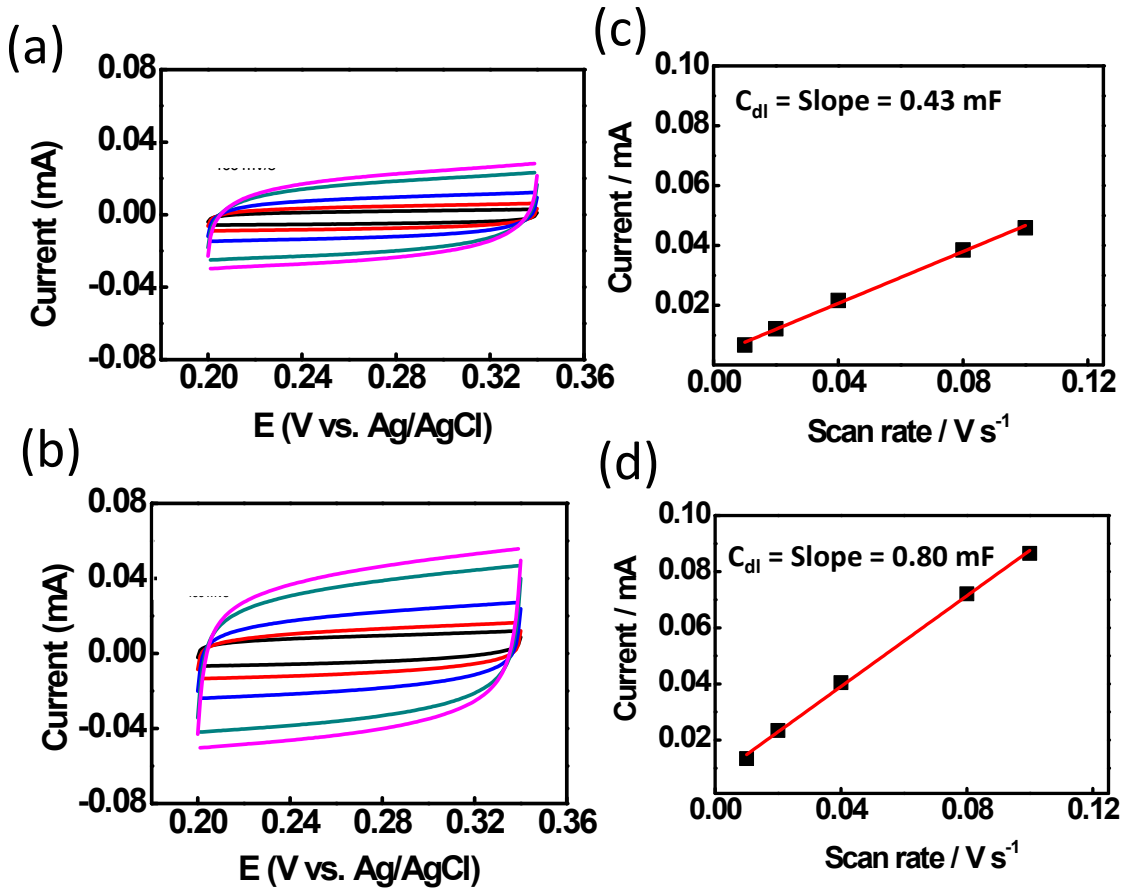

Figure S15: Static CV at multiple scan rates for (a) np-Ru and (b) Ru/C, and double-layer charging current vs scan rate for (c) np-Ru and (d) Ru/C. Scan rates are represented in black (10 V/s), red (20 V/s), blue (40 V/s), green (80 V/s), and purple (100 V/s).

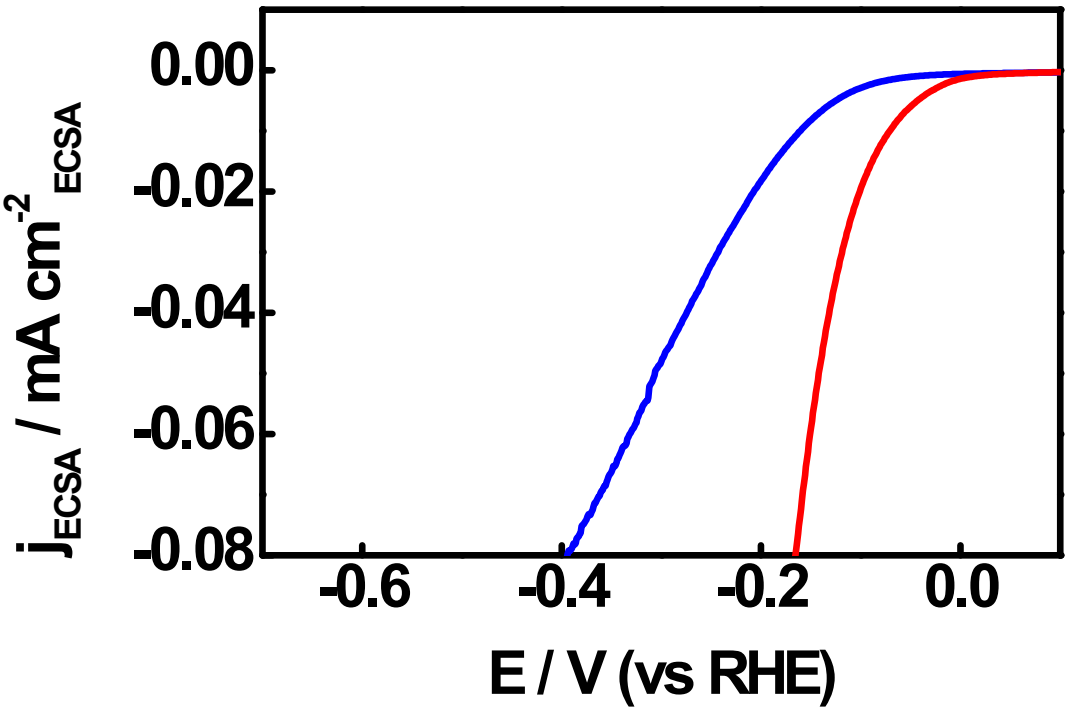

Figure S16: Linear-sweep voltammetry (LSV) profiles for np-Ru (red) and Ru/C (blue) that are normalized to the ECSA.

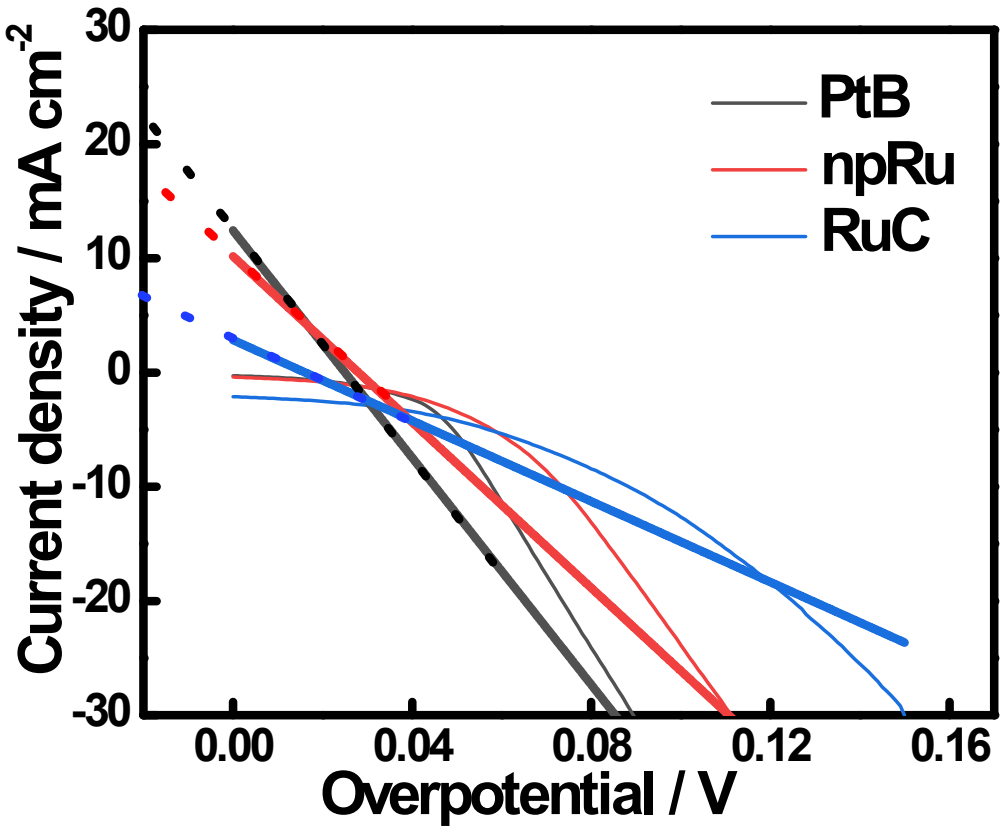

Figure S17: Determination of exchange current density (j_0) by Tafel extrapolation method.

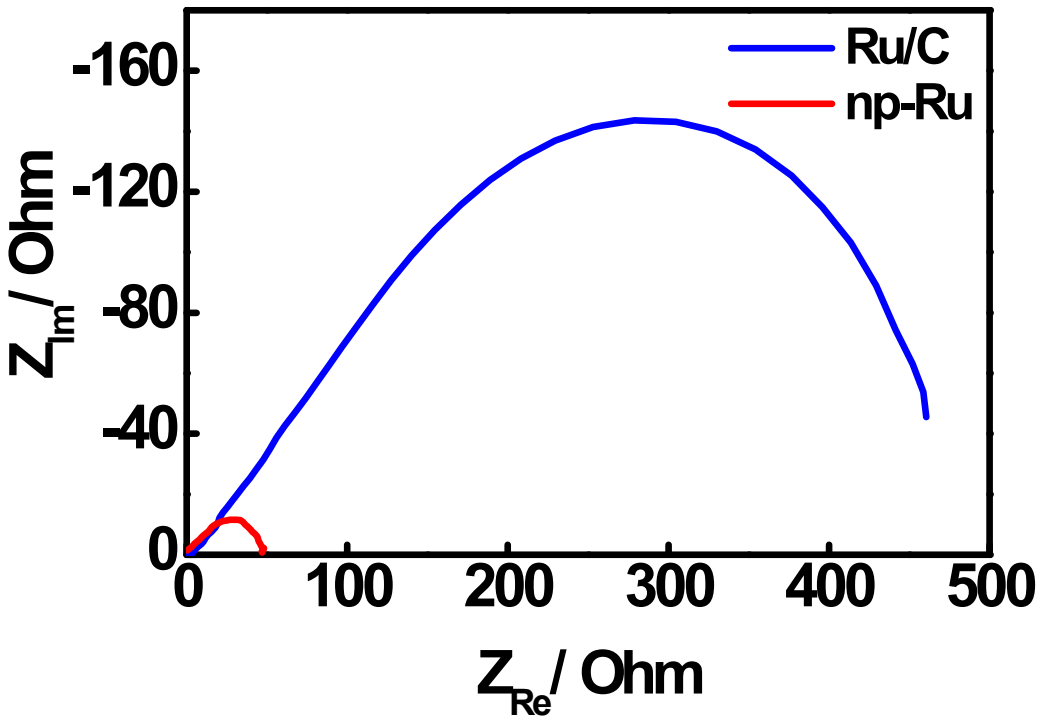

Figure 18: Electrochemical impedance spectra (EIS) at a potential of -0.4 V over the frequency range of 0.01 Hz–100 kHz in 0.5 m H_2SO_4 solution (graphite as counter electrode) for np-Ru (red), Ru/C (blue) and Pt black (black).

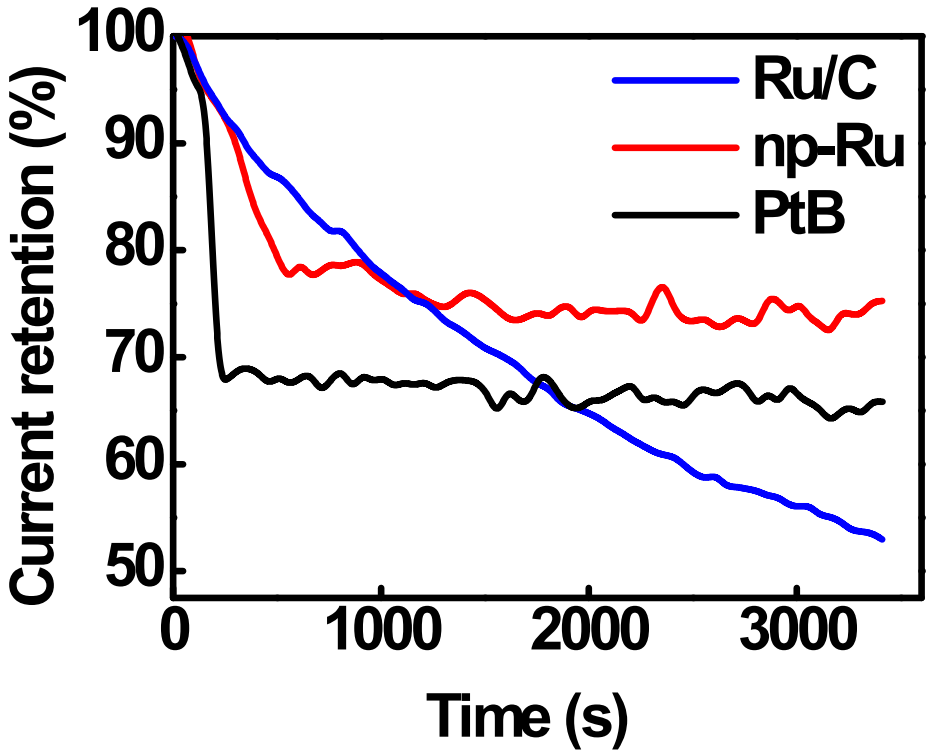

Figure 19: (a) Chronoamperometric responses collected at applied potential (-0.4 V) for 1 hour and (b) electrochemical impedance spectra (EIS) at a potential of -0.4 V over the frequency range of 0.01 Hz–100 kHz in 0.5 m H_2SO_4 solution (graphite as counter electrode) for np-Ru (red), Ru/C (blue) and Pt black (black). The current retention for PtB and np-Ru steeply dropped on the early stage because some of the catalysts came off from the electrode surface, eventually reaching plateaus.

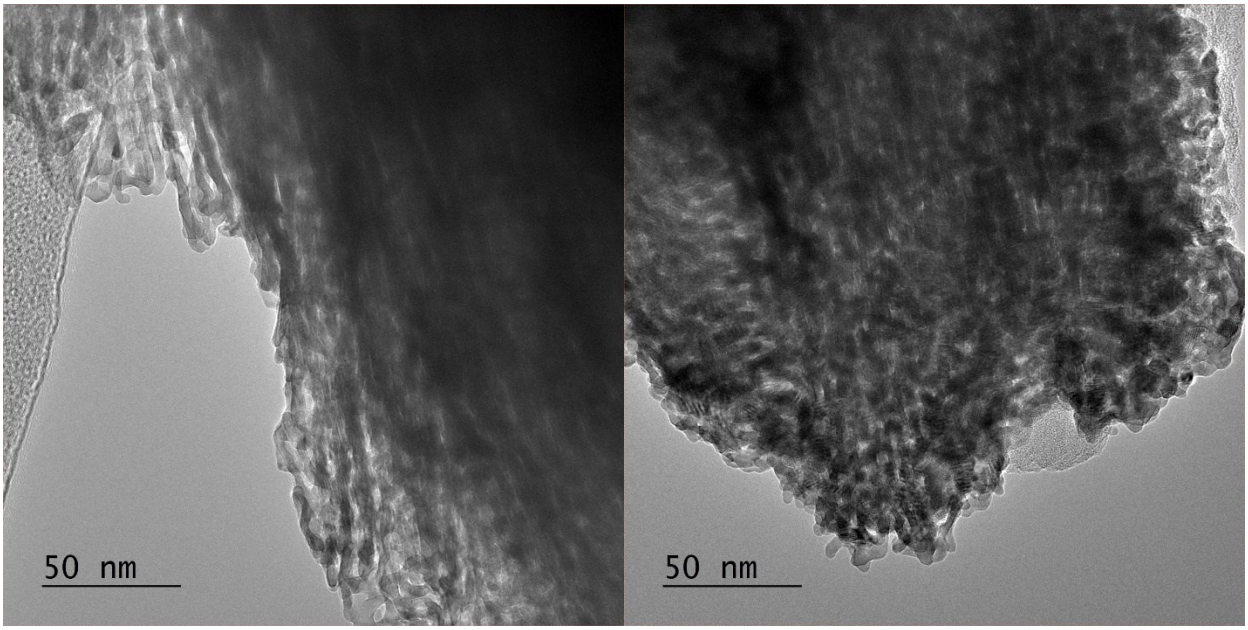

Figure S20: TEM images of as-prepared np-Ru.

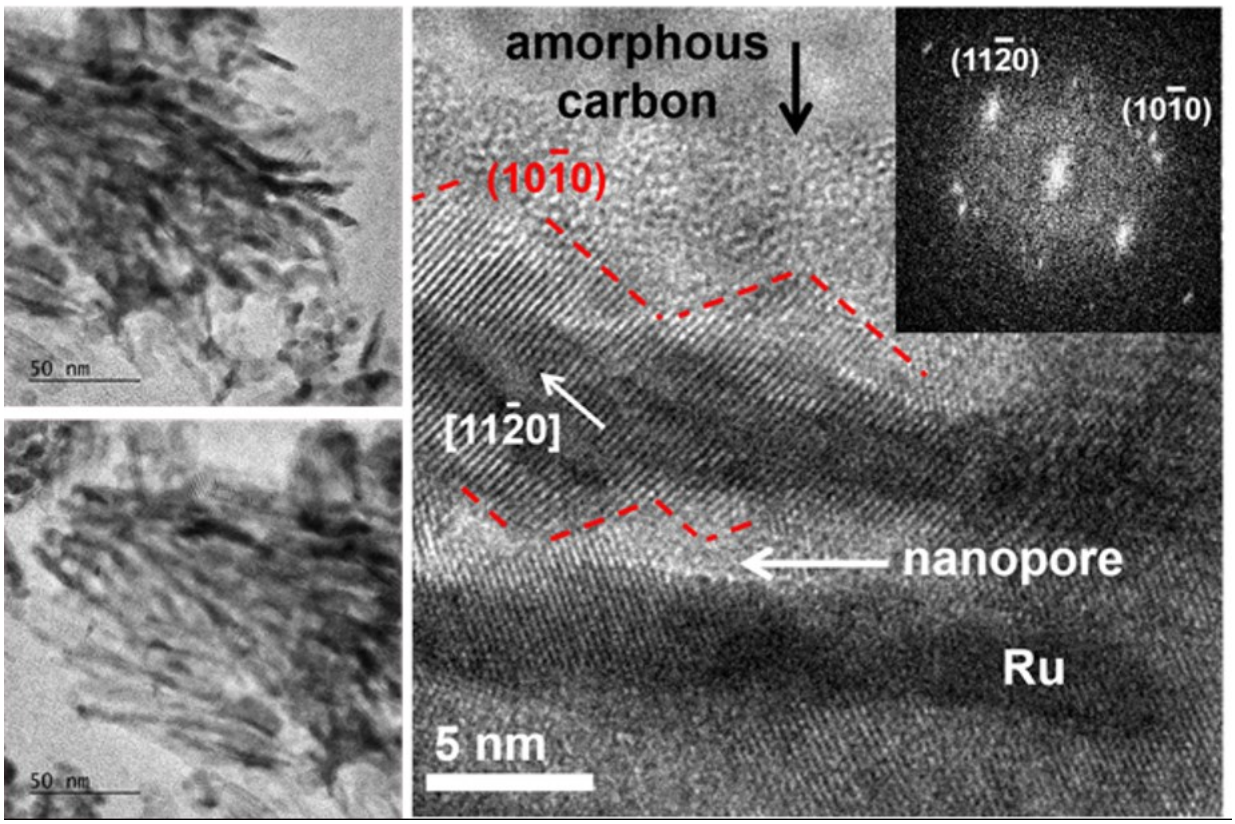

Figure S21: TEM images of np-Ru that experienced chronoamperometric tests (see Fig. S20). An FFT pattern of the right-hand side high-resolution image is presented as the inset.

References

(1) Mahmood, J.; Li, F.; Jung, S. M.; Okyay, M. S.; Ahmad, I.; Kim, S. J.; Park, N.; Jeong, H. Y.; Baek, J. B. An Efficient and PH-Universal Ruthenium-Based Catalyst for the Hydrogen Evolution Reaction. *Nat. Nanotechnol.* **2017**, *12* (5), 441–446. https://doi.org/10.1038/nnano.2016.304.

(2) Drouet, S.; Creus, J.; Collière, V.; Amiens, C.; García-Antón, J.; Sala, X.; Philippot, K. A Porous Ru Nanomaterial as an Efficient Electrocatalyst for the Hydrogen Evolution Reaction under Acidic and Neutral Conditions. *Chem. Commun.* **2017**, *53* (85), 11713–11716. https://doi.org/10.1039/c7cc05615j.

(3) McCrory, C. C. L.; Jung, S.; Ferrer, I. M.; Chatman, S. M.; Peters, J. C.; Jaramillo, T. F. Benchmarking Hydrogen Evolving Reaction and Oxygen Evolving Reaction Electrocatalysts for Solar Water Splitting Devices. *J. Am. Chem. Soc.* **2015**, *137* (13), 4347–4357. https://doi.org/10.1021/ja510442p.

(4) Zhou, Z.; Wei, L.; Wang, Y.; Karahan, H. E.; Chen, Z.; Lei, Y.; Chen, X.; Zhai, S.; Liao, X.; Chen, Y. Hydrogen Evolution Reaction Activity of Nickel Phosphide Is Highly Sensitive to Electrolyte PH. *J. Mater. Chem. A* **2017**, *5* (38), 20390–20397. https://doi.org/10.1039/c7ta06000a.

(5) Seo, B.; Baek, D. S.; Sa, Y. J.; Joo, S. H. Shape Effects of Nickel Phosphide Nanocrystals on Hydrogen Evolution Reaction. *CrystEngComm* **2016**, *18* (32), 6083–6089. https://doi.org/10.1039/c6ce00985a.

(6) Alireza, A. A.; Hamnabard, N.; Meshkati, S. M. H.; Pakan, M.; Ahn, Y. H. Effectiveness of Phase- and Morphology-Controlled MnO 2 Nanomaterials Derived from Flower-like δ-MnO 2 as Alternative Cathode Catalyst in Microbial Fuel Cells. *Dalt. Trans.* **2019**, *48* (16), 5429–5443. https://doi.org/10.1039/c9dt00520j.

(7) Gates-Rector, S.; Blanton, T. The Powder Diffraction File: A Quality Materials Characterization Database. *Powder Diffr.* **2019**, *34* (4), 352–360. https://doi.org/10.1017/S0885715619000812.

(8) Huang, C. S.; Houalla, M.; Hercules, D. M.; Kibby, C. L.; Petrakis, L. Comparison of Catalysts Derived from Oxidation of Ruthenium-Thorium (Ru3Th7) with Impregnated Ruthenium/Thoria Catalysts. *J. Phys. Chem.* **1989**, *93* (11), 4540–4544. https://doi.org/10.1021/j100348a030.

(9) Shen, J. Y.; Adnot, A.; Kaliaguine, S. An ESCA Study of the Interaction of Oxygen with the Surface of Ruthenium. *Appl. Surf. Sci.* **1991**, *51* (1–2), 47–60. https://doi.org/10.1016/0169-4332(91)90061-N.

(10) Sing, K. S. W.; Everett, D. H.; Haul, R. A. W.; Moscou, L.; Pierotti, R. A.; Rouquerol, J.; Siemieniewska, T. Reporting Physisorption Data for Gas/Solid Systems with Special Reference to the Determination of Surface Area and Porosity. *Pure Appl. Chem.* **1985**, *57* (4), 603–619. https://doi.org/10.1351/pac198557040603.